

Electromagnetic production of Σ^0 's from the proton: A new fit to recent data

Oren V. Maxwell

Department of Physics, Florida International University, Miami, Florida 33199, USA

(Received 29 October 2015; published 7 January 2016)

The reaction $ep \rightarrow e'K^+\Sigma^0$ has been investigated using a tree-level effective Lagrangian model previously employed by the author to study the $\gamma p \rightarrow K^+\Sigma^0$ reaction. In addition to the Born terms, the model incorporates a number of baryon resonances with spins up to $\frac{5}{2}$ and the two kaon resonances, $K^*(892)$ and $K_1(1270)$. Momentum and energy dependent widths for the nucleon and Δ resonances are included by means of a dynamical model that makes use of empirical on-shell branching ratios. The model parameters are fit to a large pool of photoproduction data from the CLAS and GRAAL collaborations and electroproduction data from the CLAS collaboration. Photoproduction results are presented for the unpolarized differential cross section, the photon beam asymmetry Σ , the hyperon recoil asymmetry P , and the double polarization observables C_x and C_z . Electroproduction results are presented for the virtual photoproduction structure functions σ_U , σ_{TT} , σ_{LT} , and $\sigma_{LT'}$. The photoproduction results are compared with the CLAS and GRAAL photoproduction data and with the results of an earlier fit to just the photoproduction data, while the electroproduction results are compared with both recent and older CLAS electroproduction data.

DOI: [10.1103/PhysRevC.93.014605](https://doi.org/10.1103/PhysRevC.93.014605)**I. INTRODUCTION**

The electromagnetic production of strange baryons from light nuclear targets, particularly the proton, has been a major field of interest within the nuclear physics community for several decades. The electromagnetic production of strange baryons is more difficult to study experimentally than pion electromagnetic production due to the higher energies required and the shorter lifetimes of the particles produced, and requires a more elaborate theoretical treatment due to the much larger number of resonances near the threshold for the reaction. Nevertheless, the investigation of reactions involving strange baryons is imperative for gaining a fuller understanding of the strong interaction within a nuclear environment. Most of the effort in electromagnetic strangeness production has focused on the K^+ meson Λ baryon reaction channel, but there exists enough data for the K^+ meson Σ^0 baryon reaction channel, both in photoproduction and electroproduction, to justify a separate theoretical examination of that reaction channel.

Theoretical studies of the electromagnetic production of strangeness from the proton date back to the late 1960s and early 1970s [1,2], but the theoretical work at that time was severely hampered by the lack of empirical data. There was renewed interest in the field beginning in the late 1980s [3–9] when better quality data started to become available, but, as mentioned above, this work focused mainly on Λ production. Theoretical studies that include Σ^0 production are fewer in number and generally of more recent vintage [10–17].

Recently, a fit to data from the CLAS and GRAAL collaborations was obtained for the photoproduction reaction $\gamma p \rightarrow K^+\Sigma^0$ [18]. The fit is based on a tree-level, effective Lagrangian model consisting of s -channel, u -channel, and t -channel contributions and incorporates photoproduction data from the CLAS [19–22] and GRAAL collaborations [23]. The model is similar to a model developed earlier by the author to study the electromagnetic production of Λ 's from the proton [24–28] but includes intermediate Δ resonances in the s channel, which isospin considerations prohibit in Λ

production. In this work, the fit of Ref. [18] is extended to include electroproduction data from the CLAS collaboration [29,30]. This is accomplished by incorporating form factors at the electromagnetic vertices of the model and readjusting all of the model parameters to fit the combined set of photo- and electroproduction data. Details concerning the modified model are presented in Sec. II.

The fitted data includes CLAS photoproduction data for the unpolarized differential cross section [20,22], the hyperon recoil asymmetry [19,22], and a pair of double polarization observables [21]; GRAAL photoproduction data for the photon beam asymmetry [23]; and CLAS electroproduction data for the virtual photon structure functions σ_U , σ_{TT} , σ_{LT} , and $\sigma_{LT'}$ [29,30]. Due to the relatively large number of parameters involved in strangeness electroproduction, the fitting was accomplished in a two step procedure that is described in Sec. III.

Section IV contains the results of the fit and provides a comparison of the calculated observables with the data for a variety of kinematical situations. The photoproduction observables are also compared with results obtained with the fit of Ref. [18].

II. REACTION MODEL

The contributions to the reaction model for electromagnetic strangeness production in a tree-level effective Lagrangian model can be divided into three basic types according to whether the squared four-momentum in the intermediate state propagator corresponds to the s , t , or u Mandelstaam variable. These are illustrated in Fig. 1. In each channel, the Born terms are supplemented with terms involving the excitation of intermediate hadronic resonances appropriate to that channel.

Table I lists all of the baryon resonances that have been incorporated in the model. In the s channel, these include all of the well established nucleon and Δ resonances (three and four star statuses in the particle data tables [31]) with spins less than or equal to $\frac{5}{2}$ and three additional two star residences, the

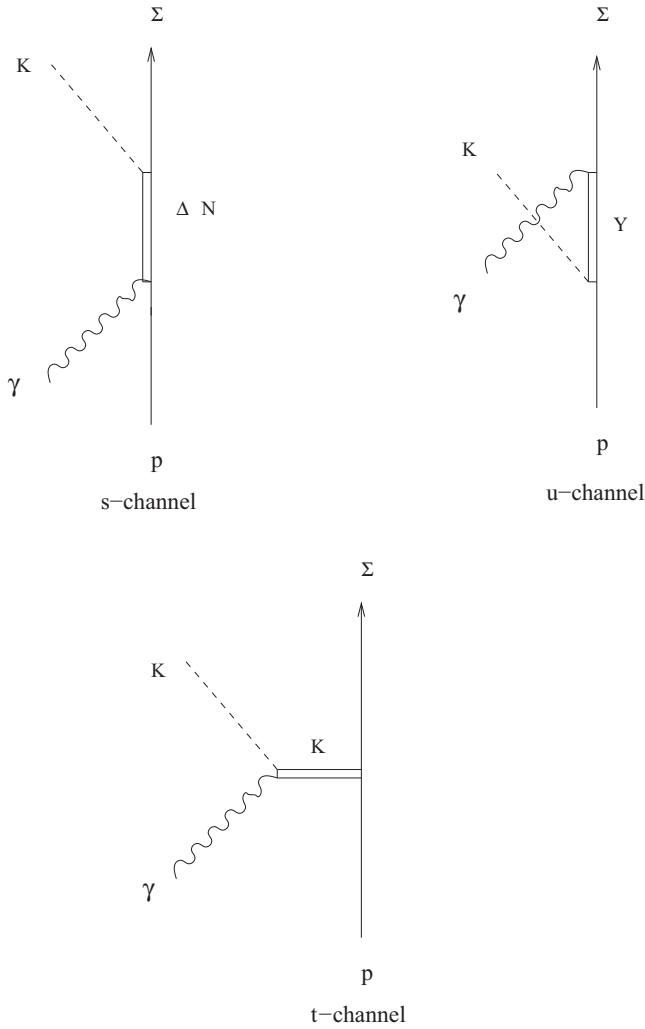


FIG. 1. Contributions to the reaction amplitude.

$N(1860)$, $N(1880)$, and $N(2000)$ resonances. The inclusion of these less well-established resonances of higher energy improves the fit at the higher energy end. Several other two star nucleon and Δ resonances that appear in the data tables have not been included in the fit since there is no evidence for these resonances in the most recent George Washington University analysis.

In the u channel, the resonances included are the same as those incorporated in the earlier fits to Λ production data [26–28]. In Ref. [26], it was shown that the inclusion of more resonances in the u channel does not materially improve the fits. I have also employed the same t -channel kaon resonances that were incorporated in the Λ production fits, namely, the $K^*(892)$ and the $K_1(1270)$ resonances.

The s -, u -, and t -channel contributions to the photoproduction reaction amplitude in the impulse approximation are discussed in Ref. [18]. The corresponding electroproduction matrix element of the reaction amplitude \hat{T} between initial state I and final state F can be expressed as

$$\langle F | \hat{T} | I \rangle = \frac{l_\mu h^\mu}{q^2}, \quad (1)$$

 TABLE I. Baryon resonances included in the model. J^P refers to the spin and parity of the resonance.

Resonance	J^P
$N(1440)$	$\frac{1}{2}^+$
$N(1520)$	$\frac{3}{2}^-$
$N(1535)$	$\frac{1}{2}^-$
$N(1650)$	$\frac{1}{2}^-$
$N(1675)$	$\frac{3}{2}^-$
$N(1680)$	$\frac{5}{2}^+$
$N(1700)$	$\frac{3}{2}^-$
$N(1710)$	$\frac{1}{2}^+$
$N(1720)$	$\frac{3}{2}^+$
$N(1860)$	$\frac{5}{2}^+$
$N(1875)$	$\frac{3}{2}^-$
$N(1880)$	$\frac{1}{2}^+$
$N(1900)$	$\frac{3}{2}^+$
$N(2000)$	$\frac{5}{2}^+$
$\Delta(1232)$	$\frac{3}{2}^+$
$\Delta(1600)$	$\frac{3}{2}^+$
$\Delta(1620)$	$\frac{1}{2}^-$
$\Delta(1700)$	$\frac{3}{2}^-$
$\Delta(1905)$	$\frac{5}{2}^+$
$\Delta(1910)$	$\frac{1}{2}^+$
$\Delta(1920)$	$\frac{3}{2}^+$
$\Delta(1930)$	$\frac{5}{2}^-$
$\Lambda(1405)$	$\frac{1}{2}^-$
$\Lambda(1670)$	$\frac{1}{2}^-$
$\Lambda(1820)$	$\frac{5}{2}^+$
$\Lambda(1830)$	$\frac{3}{2}^-$
$\Lambda(1890)$	$\frac{3}{2}^+$
$\Lambda(2110)$	$\frac{5}{2}^+$
$\Sigma(1385)$	$\frac{3}{2}^+$
$\Sigma(1775)$	$\frac{5}{2}^-$
$\Sigma(1915)$	$\frac{5}{2}^+$
$\Sigma(1940)$	$\frac{3}{2}^-$

where q is the virtual photon four-momentum, l_μ is the lepton current given by

$$l_\mu = e \bar{u}_{M'}(p') \gamma_\mu u_M(p), \quad (2)$$

with p (p') and M (M') denoting the incident (final) electron four-momentum and spin projection, respectively, and h^μ is the hadron current given by

$$h^\mu = e \bar{u}_{M_\Sigma}(p_\Sigma) \hat{t}^\mu u_{M_p}(p_p). \quad (3)$$

The form of the hadronic amplitude, \hat{t}^μ , appearing in the last expression depends upon the channel considered. In particular, for the s , u , and t channels, the appropriate expressions are

$$\hat{t}_s^\mu = \sum_{N^*} [\mathcal{V}_K^\dagger(p_K) D(p_s) \mathcal{V}_\gamma(q)]^\mu, \quad (4)$$

$$\hat{t}_u^\mu = \sum_{Y^*} [\mathcal{V}_\gamma^\dagger(q) D(p_u) \mathcal{V}_K(p_K)]^\mu, \quad (5)$$

and

$$\hat{t}_t^\mu = \sum_{K^*} [\mathcal{V}_{\gamma K}^\dagger(q, p_t) D_t(p_t) \mathcal{V}_{p\Sigma}(p_t)]^\mu, \quad (6)$$

where q is the virtual photon four-momentum, and $p_s = p_\Sigma + p_K$, $p_u = p_\Sigma - q$, and $p_t = q - p_K$. The \mathcal{V} 's here are the vertex functions at the electromagnetic and strong interaction vertices, and the D 's are the intermediate hadron propagators. Note that the sums include both Born and resonance contributions.

The vertex functions and propagators in these expressions depend upon the spins and parities of the intermediate baryons. The propagators are identical to those employed in Ref. [18]; the reader is referred to that reference for the specific forms. The interaction vertices are also very similar to those employed in Ref. [18], but modified to treat electroproduction, rather than photoproduction. They are listed below.

In the s and u channels, the positive parity electromagnetic interaction vertices appropriate for electroproduction are given (with form factors suppressed) by

$$\begin{aligned} \mathcal{V}_{\gamma \frac{1}{2}^+}^\mu(q) &= \frac{e\kappa}{2m_B} i\sigma^{\mu\nu} q_\nu, \\ \mathcal{V}_{\gamma \frac{3}{2}^+}^{\mu\nu}(q) &= \left[\frac{g_1}{2m_B} (\gamma \cdot q g^{\mu\nu} - \gamma^\mu q^\nu) \right. \\ &\quad \left. + \frac{g_2}{4m_B^2} (p_B^\mu q^\nu - q \cdot p_B g^{\mu\nu}) \right] \gamma_5, \quad (7) \\ \mathcal{V}_{\gamma \frac{5}{2}^+}^{\mu\nu\alpha}(q) &= \left[\frac{g_1}{2m_B} (\gamma \cdot q g^{\mu\nu} - \gamma^\mu q^\nu) \right. \\ &\quad \left. + \frac{g_2}{4m_B^2} (p_B^\mu q^\nu - q \cdot p_B g^{\mu\nu}) \right] q^\alpha, \end{aligned}$$

where m_B and p_B are the mass and four-momentum, respectively, of the incident proton in the s channel and the mass and four-momentum, respectively, of the outgoing Σ in the u channel, and $g^{\mu\nu}$ denotes the elements of the 4 dimensional metric tensor. In the expression for the spin $\frac{1}{2}$ vertex, κ is defined by its relation to the transition magnetic moment,

$$\mu_T = \frac{e\kappa}{m_B + m_I}, \quad (8)$$

where m_I is the mass of the intermediate baryon. The Born terms in both channels have an additional charge contribution given by

$$\mathcal{V}_{\text{charge}}^\mu = e\gamma^\mu. \quad (9)$$

Note that in photoproduction, which involves a physical photon, current conservation requires that the charge contribution in the u channel vanish because the outgoing Σ is neutral.

Thus in electroproduction, the form factor that multiplies the u -channel charge contribution must vanish when the incident photon is on shell.

In the t channel, the positive parity electromagnetic interaction vertices are given (again with form factors suppressed) by

$$\begin{aligned} \mathcal{V}_{\gamma K}^\mu &= e(2p_K^\mu - q^\mu), \\ \mathcal{V}_{\gamma K(892)}^{\mu\nu} &= \frac{g_{\gamma K K^*}}{m_{sc}} \epsilon^{\mu\alpha\beta\nu} q_\alpha p_{t\beta}, \quad (10) \\ \mathcal{V}_{\gamma K(1270)}^{\mu\nu} &= \frac{g_{\gamma K K^*1}}{m_{sc}} (p_t^\mu q^\nu - q \cdot p_t g^{\mu\nu}), \end{aligned}$$

where ϵ is the totally antisymmetric tensor of rank 4, p_t is the four-momentum of the intermediate kaon or kaon resonance, and m_{sc} is a scaling mass, set equal to 1 GeV, introduced to make the electromagnetic coupling strengths dimensionless.

The corresponding expressions for the strong interaction vertices are

$$\begin{aligned} \mathcal{V}_{K \frac{1}{2}^+}(p_K) &= g\gamma_5, \\ \mathcal{V}_{K \frac{3}{2}^+}^\mu(p_K) &= -\frac{g}{m_\pi} p_K^\mu, \quad (11) \\ \mathcal{V}_{K \frac{5}{2}^+}^{\mu\nu}(p_K) &= \frac{g}{m_\pi^2} p_K^\mu p_K^\nu \gamma_5 \end{aligned}$$

in the s and u channels for positive parity intermediate baryons and

$$\begin{aligned} \mathcal{V}_{p\Sigma K} &= g_{\Sigma K p} \gamma_5, \\ \mathcal{V}_{p\Sigma K(892)}^\mu &= \left(g_{\Sigma K^* p}^V + \frac{g_{\Sigma K^* p}^T}{m_p + m_\Sigma} \gamma \cdot p_t \right) \gamma^\mu, \quad (12) \\ \mathcal{V}_{p\Sigma K(1270)}^\mu &= \left(g_{\Sigma K 1 p}^V + \frac{g_{\Sigma K 1 p}^T}{m_p + m_\Sigma} \gamma \cdot p_t \right) \gamma^\mu \gamma_5 \end{aligned}$$

in the t channel, where the V and T superscripts on the coupling strengths refer to the vector and tensor contributions. In the s and u channels the interaction vertices for negative parity intermediate baryons are just the positive parity expressions with the γ_5 factor transposed from the strong interaction vertex to the electromagnetic vertex.

In the u and t channels, the intermediate squared four-momenta are small or negative so that the intermediate resonances in those channels cannot decay. By contrast, p_s^2 is generally large enough that one or more decay channels are open for the intermediate nucleon and Δ resonances in the s channel. Thus, s -channel propagators must include widths, and these widths are both energy and momentum dependent. In earlier work involving the photoproduction of Λ 's, a dynamical model was developed by the author to treat the energy and momentum dependence of the widths [24,26]. The model was also employed in Ref. [18], where a brief description of the model can be found, and is employed in the present fit for those s -channel resonances where there is sufficient branching ratio data to make reasonable estimates of the on-shell partial decay widths. This is generally the case for most of the well-established nucleon and Δ resonances, but for the two star nucleon resonances included in the fit, the

available branching ratio data is too sparse to make use of the model. Hence, for these resonances, a fixed width, equal to the on-shell width given in the particle tables, is employed. Further details concerning the widths may be found in Ref. [18].

In electroproduction, the exchanged photon is off shell. Thus, in an effective Lagrangian treatment of the reaction amplitude, it is necessary to include form factors at the electromagnetic vertices. Moreover, the form factors must be chosen so that the current conservation condition,

$$q_\mu h^\mu = 0, \quad (13)$$

is satisfied. In this work, I adopt the same form factor prescription as was employed in the earlier studies of Λ electroproduction [27,28]. For the proton, the charge and magnetic form factors derived by Gari and Krumpelmann [32] using a modified vector dominance model are employed.

For the u -channel Born contribution, involving an intermediate Σ , the charge and magnetic form factors are expressed as linear combinations of two other form factors through the relations

$$F_C(q^2) = F_{\Sigma 1}(q^2) - \tau_\Sigma F_{\Sigma 2}(q^2), \quad (14)$$

$$F_M(q^2) = \frac{1}{\kappa_\Sigma} [F_{\Sigma 1}(q^2) + F_{\Sigma 2}(q^2)],$$

with

$$\tau_\Sigma = \frac{q^2}{4m_\Sigma^2} \quad (15)$$

and

$$\begin{aligned} F_{\Sigma 1}(q^2) &= \frac{1}{2} [F_1(q^2) - F_2(q^2)], \\ F_{\Sigma 2}(q^2) &= \frac{\kappa_\Sigma}{2} [F_1(q^2) + F_2(q^2)]. \end{aligned} \quad (16)$$

The form factors F_1 and F_2 are assumed to have the same functional form,

$$F_i(q^2) = \frac{1}{1 + \alpha_i} \frac{\Lambda_i^2}{\Lambda_i^2 - q^2} \left(1 + \alpha_i \frac{\Lambda_i^2}{\Lambda_i^2 - q^2} \right), \quad (17)$$

but with different values for the parameters α_i and Λ_i . The remaining s - and u -channel contributions require just a single magnetic form factor, which is chosen to have the same functional form as that given by Eq. (17).

For the t -channel Born contribution, I make use of a parametrization motivated by the relativistic quark model [33] which is given by

$$F_K(q^2) = \alpha_K \frac{\Lambda_1^2}{\Lambda_1^2 - q^2} + (1 - \alpha_K) \left(\frac{\Lambda_2^2}{\Lambda_2^2 - q^2} \right)^2, \quad (18)$$

with $\alpha_K = 0.398$, $\Lambda_1 = 0.642$, and $\Lambda_2 = 1.386$ GeV. The remaining t -channel form factors are parameterized through

the relation

$$F_{K^*}(q^2) = \frac{\Lambda_{K^*}^2}{\Lambda_{K^*}^2 - q^2}. \quad (19)$$

To preserve current conservation in the Born terms, it is necessary to modify the charge contributions to the hadronic amplitudes when form factors are included. The modified charge contributions are given by

$$\begin{aligned} \hat{t}_{s,ch}^\mu &= e F_C(q^2) \gamma^\mu + e [1 - F_C(q^2)] \frac{q^\mu}{q^2} \gamma \cdot q, \\ \hat{t}_{u,ch}^\mu &= e F_C(q^2) \left[\gamma^\mu - \frac{q^\mu}{q^2} \gamma \cdot q \right], \\ \hat{t}_{t,ch}^\mu &= e F_K(q^2) (2p_K^\mu - q^\mu) \\ &\quad + e [1 - F_K(q^2)] \left(\frac{2p_K \cdot q}{q^2} - 1 \right) q^\mu. \end{aligned} \quad (20)$$

III. FITTING PROCEDURE

As mentioned previously, the fitted photoproduction observables consist of the unpolarized differential cross section, the photon beam asymmetry Σ , the hyperon recoil asymmetry P , and a pair of double polarization parameters, C_x and C_z . The differential cross section is given in the center of mass (c.m.) by the expression

$$\frac{d\sigma}{d\Omega} = \frac{1}{(2\pi)^2} \frac{m_p m_\Sigma p_F}{4E_\gamma s} \frac{1}{4} \sum_{\text{spins}} |(F|\hat{T}|I)|^2, \quad (21)$$

where p_F is the outgoing three-momentum magnitude, s the squared c.m. energy, and E_γ the incident photon energy. The single polarization observables are defined by the relations

$$\Sigma = \frac{d\sigma_\gamma^\perp - d\sigma_\gamma^\parallel}{d\sigma_\gamma^\perp + d\sigma_\gamma^\parallel} \quad (22)$$

and

$$P = \frac{d\sigma_\Sigma^+ - d\sigma_\Sigma^-}{d\sigma_\Sigma^+ + d\sigma_\Sigma^-}, \quad (23)$$

where the superscripts \perp and \parallel refer to photon polarizations perpendicular and parallel, respectively, to the scattering plane, and the superscripts $+$ and $-$ refer to Σ spin projections above and below, respectively, the scattering plane. The double polarization variables are defined for circularly polarized photons with positive helicity by the relation

$$C_i = \frac{d\sigma_\Sigma^+ - d\sigma_\Sigma^-}{d\sigma_\Sigma^+ + d\sigma_\Sigma^-}, \quad (24)$$

where now the superscripts $+$ and $-$ refer to Σ spin projections along and opposite, respectively, to either the z ($i = z$) or x ($i = x$) axes.

For the electroproduction reaction, the fitted observables consist of the structure functions defined by the virtual photoproduction cross section in experiments where the incident

TABLE II. Coupling strength products. The first column of numbers is from fit 2 of Ref. [18]; the second column is from the fit described here.

Spin $\frac{1}{2}$ resonances			
$N(1440)$	F_{N^*}	-7.8671	-9.2689
$N(1535)$	F_{N^*}	1.1034	1.8246
$N(1650)$	F_{N^*}	-0.0343	0.1467
$N(1710)$	F_{N^*}	-0.0674	-0.2294
$N(1880)$	F_{N^*}	1.0145	0.7439
$\Delta(1620)$	F_Δ	-0.7896	-1.0283
$\Delta(1910)$	F_Δ	-1.4869	-1.1084
$\Lambda(1405)$	F_{Λ^*}	2.2330	-1.1230
$\Lambda(1670)$	F_{Λ^*}	0.0111	7.0034
Spin $\frac{3}{2}$ resonances			
$N(1520)$	$G_{N^*}^1$	2.0474	4.6247
	$G_{N^*}^2$	2.6298	1.1879
$N(1700)$	$G_{N^*}^1$	-2.8002	0.2886
	$G_{N^*}^2$	-4.1911	-1.2629
$N(1720)$	$G_{N^*}^1$	0.2572	-0.2732
	$G_{N^*}^2$	-0.4442	0.0751
$N(1875)$	$G_{N^*}^1$	-0.9594	-0.5314
	$G_{N^*}^2$	-1.0823	-0.7026
$N(1900)$	$G_{N^*}^1$	0.1035	-0.0917
	$G_{N^*}^2$	0.0647	0.1024
$\Delta(1232)$	G_Δ^1	0.0870	-0.4396
	G_Δ^2	-0.5610	-0.5299
$\Delta(1600)$	G_Δ^1	-0.9305	0.7074
	G_Δ^2	3.1898	1.0057
$\Delta(1700)$	G_Δ^1	6.2298	-0.6947
	G_Δ^2	8.9796	5.2056
$\Delta(1920)$	G_Δ^1	-0.1417	0.0620
	G_Δ^2	-0.0074	-0.0574
$\Lambda(1890)$	$G_{\Lambda^*}^1$	-7.3739	-4.6591
	$G_{\Lambda^*}^2$	6.6918	-2.4737
$\Sigma(1385)$	$G_{\Sigma^*}^1$	3.1159	0.6676
	$G_{\Sigma^*}^2$	-5.4446	-0.7329
$\Sigma(1940)$	$G_{\Sigma^*}^1$	6.1471	1.3131
	$G_{\Sigma^*}^2$	9.7442	3.1860
Spin $\frac{5}{2}$ resonances			
$N(1675)$	$G_{N^*}^1$	0.0080	0.0094
	$G_{N^*}^2$	0.0110	0.0034
$N(1680)$	$G_{N^*}^1$	-0.0993	-0.0839
	$G_{N^*}^2$	-0.1965	-0.1979
$N(1860)$	$G_{N^*}^1$	-0.0608	-0.0327
	$G_{N^*}^2$	-0.0924	-0.0687
$N(2000)$	$G_{N^*}^1$	-0.0104	0.0014
	$G_{N^*}^2$	-0.0129	0.0011
$\Delta(1905)$	G_Δ^1	0.0974	0.0551

TABLE II. (Continued.)

	G_Δ^2	0.1695	0.1297
$\Delta(1930)$	G_Δ^1	-0.0002	-0.0031
	G_Δ^2	-0.0022	-0.0035
$\Lambda(1820)$	$G_{\Lambda^*}^1$	0.1079	0.1362
	$G_{\Lambda^*}^2$	0.1811	-0.0977
$\Lambda(1830)$	$G_{\Lambda^*}^1$	0.0458	-0.0189
	$G_{\Lambda^*}^2$	-0.6987	-1.4837
$\Lambda(2110)$	$G_{\Lambda^*}^1$	-0.1345	0.0305
	$G_{\Lambda^*}^2$	-0.2581	-0.1719
$\Sigma(1775)$	$G_{\Sigma^*}^1$	-0.0567	-0.0150
	$G_{\Sigma^*}^2$	0.6461	1.3998
$\Sigma(1915)$	$G_{\Sigma^*}^1$	0.0585	-0.1651
	$G_{\Sigma^*}^2$	0.1698	0.2760
Kaon resonances			
$K(892)$	$G_{K^*}^V$	8.6461	5.7942
	$G_{K^*}^T$	2.1909	-0.9099
$K(1270)$	$G_{K^*}^V$	11.9499	11.3408
	$G_{K^*}^T$	3.7975	5.2725

electron helicity is measured. This is given by

$$\frac{d\sigma_\gamma}{d\Omega_K} = \sigma_T + \epsilon\sigma_L + \epsilon\sigma_{TT} \cos 2\phi + \sqrt{\epsilon(1+\epsilon)}\sigma_{LT} \cos \phi + \mathcal{H}\sqrt{\epsilon(1-\epsilon)}\sigma_{LT'} \sin \phi, \quad (25)$$

where ϕ is the angle between the hadron and lepton planes in electroproduction, \mathcal{H} is the incident electron helicity, and ϵ is the transverse polarization of the virtual photon,

$$\epsilon = \left(1 - 2\frac{\mathbf{q}^2}{q^2} \tan^2 \frac{\Psi}{2}\right)^{-1}, \quad (26)$$

with \mathbf{q} denoting the spatial part of the virtual photon momentum and Ψ the electron scattering angle in the laboratory frame.

The structure functions are related to the hadronic matrix elements in electroproduction h^μ defined previously through the expressions

$$\begin{aligned} \sigma_T &= \frac{1}{4}k \sum_{M_\Sigma M_p} (|h_x|^2 + |h_y|^2), \\ \sigma_L &= \frac{1}{2}k \sum_{M_\Sigma M_p} \frac{-q^2}{q_0^2} |h_z|^2, \\ \sigma_{TT} &= \frac{1}{4}k \sum_{M_\Sigma M_p} (|h_x|^2 - |h_y|^2), \\ \sigma_{LT} &= -\frac{1}{2}k \sum_{M_\Sigma M_p} \frac{1}{q_0} \sqrt{-2q^2} \text{Re}(h_x h_z^*), \\ \sigma_{LT'} &= -\frac{1}{2}k \sum_{M_\Sigma M_p} \frac{1}{q_0} \sqrt{-2q^2} \text{Im}(h_x h_z^*), \end{aligned} \quad (27)$$

TABLE III. Fit results for the electromagnetic form factor parameters.

Spin $\frac{1}{2}$ resonances		
	Λ	α
$N(1440)$	0.3123	4.8705
$N(1535)$	0.4613	4.5155
$N(1650)$	0.9745	-4.8632
$N(1710)$	1.2093	0.3237
$N(1880)$	1.2481	4.5044
$\Delta(1620)$	0.4242	0.0001
$\Delta(1910)$	0.5655	-4.1001
Λ	0.2310	1.8426
$\Lambda(1405)$	0.7271	-0.0007
$\Lambda(1670)$	0.7522	4.8858
$F_1(\Sigma)$	0.3941	3.9348
$F_2(\Sigma)$	0.5502	0.2432
Spin $\frac{3}{2}$ resonances		
	Λ	α
$N(1520)$	0.2240	0.3628
$N(1700)$	0.2478	-4.3257
$N(1720)$	1.0137	2.8480
$N(1875)$	0.2591	-0.8346
$N(1900)$	0.7648	3.5602
$\Delta(1232)$	0.5597	0.0007
$\Delta(1600)$	0.2241	-0.9078
$\Delta(1700)$	0.2900	4.3555
$\Delta(1920)$	1.7310	-4.3353
$\Lambda(1890)$	0.2026	1.2665
$\Sigma(1385)$	0.2006	-0.6737
$\Sigma(1940)$	0.2521	2.9120
Spin $\frac{5}{2}$ resonances		
	Λ	α
$N(1675)$	0.3835	-0.0778
$N(1680)$	0.2104	0.7383
$N(1860)$	0.2288	0.6092
$N(2000)$	1.2381	-2.5632
$\Delta(1905)$	0.3512	4.0883
$\Delta(1930)$	1.3354	-3.9426
$\Lambda(1820)$	0.3828	2.1829
$\Lambda(1830)$	0.2096	4.6589
$\Lambda(2110)$	0.5462	2.3219
$\Sigma(1775)$	0.2019	4.9830
$\Sigma(1915)$	0.5033	3.6883
t -channel resonances		
	Λ_{K^*}	
$K(892)$	0.219	
$K(1270)$	0.208	

with

$$k = \frac{m_p m_\Sigma p_K}{16\pi^2 |\mathbf{q}| s}, \quad (28)$$

where q_0 is the time component of the virtual four-momentum, and s is the square of the $K\Sigma$ c.m. energy.

One of the main advantages of the expansion given by Eq. (25) is that all of the dependence on the kinematic variables ϕ and ϵ has been factored out of the structure functions, so that these observables can be examined as functions of just

the three variables q^2 , the $K\Sigma$ c.m. energy, and the c.m. kaon scattering angle. In practice, the difficulty in separating the longitudinal and transverse structure functions experimentally means that there is very little data for these two functions separately. Instead, the available data is for the combination,

$$\sigma_U = \sigma_T + \epsilon\sigma_L, \quad (29)$$

which depends on the incident electron energy through the variable ϵ .

The fits were carried out by minimizing the χ^2 per degree of freedom defined by the relation

$$\frac{\chi^2}{\nu} = \sum \frac{(Y_{\text{calc}} - Y_{\text{exp}})^2}{\sigma^2}, \quad (30)$$

where the sum is over the data points employed in the fit, Y_{calc} and Y_{exp} are calculated and measured values, respectively, for a particular observable, and σ^2 is the squared uncertainty in Y_{exp} . The number of degrees of freedom in the fit is given by $\nu = N_{\text{data}} - N_{\text{par}}$, where N_{data} is the number of data points and N_{par} the number of fit parameters. The photoproduction data have been fit from threshold up to a c.m. energy of 2.2 GeV,

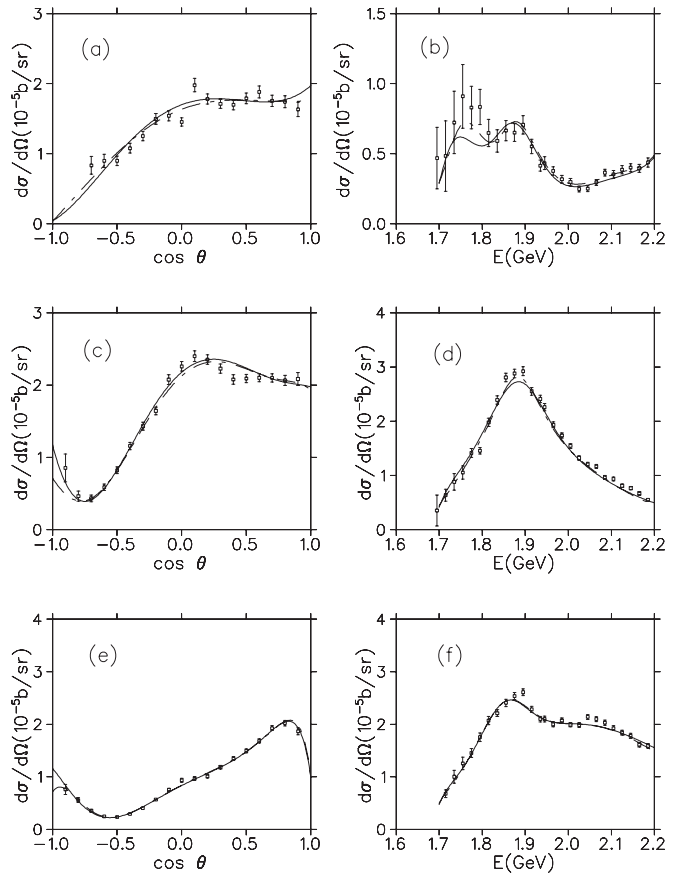


FIG. 2. Differential cross section vs. $\cos\theta_{c.m.}$ for (a) $E_{c.m.} = 1.795$, (c) $E_{c.m.} = 1.945$, and (e) $E_{c.m.} = 2.105$ GeV; differential cross section vs. $E_{c.m.}$ for (b) $\cos\theta_{c.m.} = -0.7$, (d) $\cos\theta_{c.m.} = 0$, and (f) $\cos\theta_{c.m.} = 0.7$. The solid curves were obtained with the fit described here and the dot-dashed curves with fit 2 of Ref. [18]. Data are from Refs. [20,22].

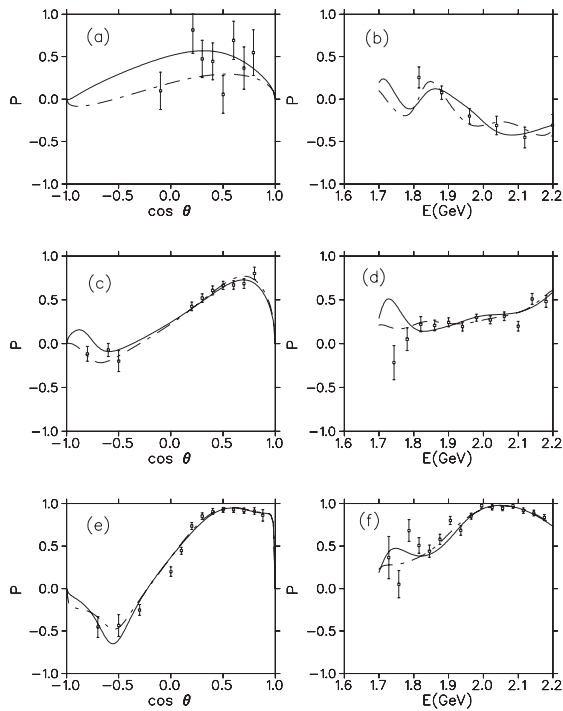


FIG. 3. Hyperon recoil asymmetry vs. $\cos \theta_{c.m.}$ for (a) $E_{c.m.} = 1.729$, (c) $E_{c.m.} = 1.933$, and (e) $E_{c.m.} = 2.111$ GeV; hyperon recoil asymmetry vs. $E_{c.m.}$ for (b) $\cos \theta_{c.m.} = -0.7$, (d) $\cos \theta_{c.m.} = 0$, and (f) $\cos \theta_{c.m.} = 0.7$. The solid curves were obtained with the fit described here and the dot-dashed curves with fit 2 of Ref. [18]. Data are from Refs. [19,22].

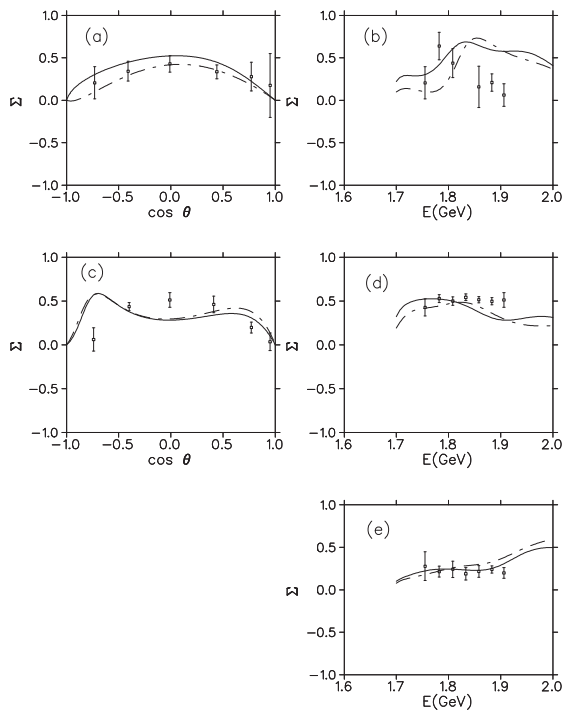


FIG. 4. Photon beam asymmetry vs. $\cos \theta_{c.m.}$ for (a) $E_{c.m.} = 1.755$, and (c) $E_{c.m.} = 1.906$ GeV; photon beam asymmetry vs. $E_{c.m.}$ for (b) $\cos \theta_{c.m.} = -0.73$, (d) $\cos \theta_{c.m.} = 0$, and (e) $\cos \theta_{c.m.} = 0.77$. The solid curves were obtained with the fit described here and the dot-dashed curves with fit 2 of Ref. [18]. Data are from Ref. [23].

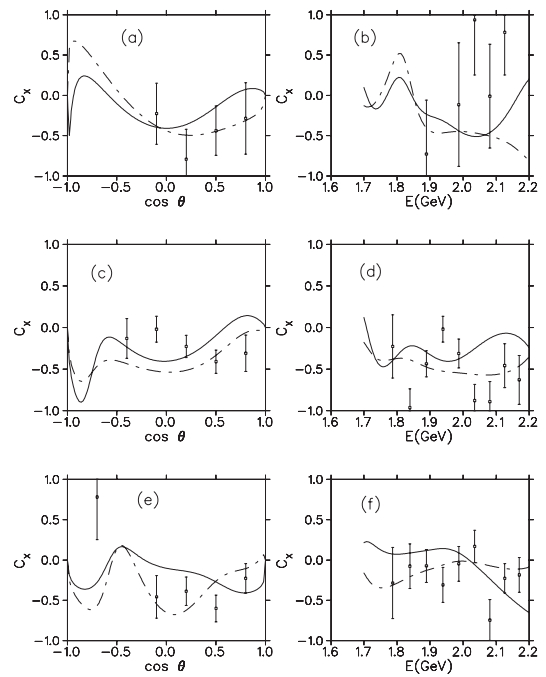


FIG. 5. Double polarization parameter C_X vs. $\cos \theta_{c.m.}$ for (a) $E_{c.m.} = 1.787$, (c) $E_{c.m.} = 1.939$, and (e) $E_{c.m.} = 2.126$ GeV; double polarization parameter C_X vs. $E_{c.m.}$ for (b) $\cos \theta_{c.m.} = -0.7$, (d) $\cos \theta_{c.m.} = -0.1$, and (f) $\cos \theta_{c.m.} = 0.8$. The solid curves were obtained with the fit described here and the dot-dashed curves with fit 2 of Ref. [18]. Data are from Ref. [21].

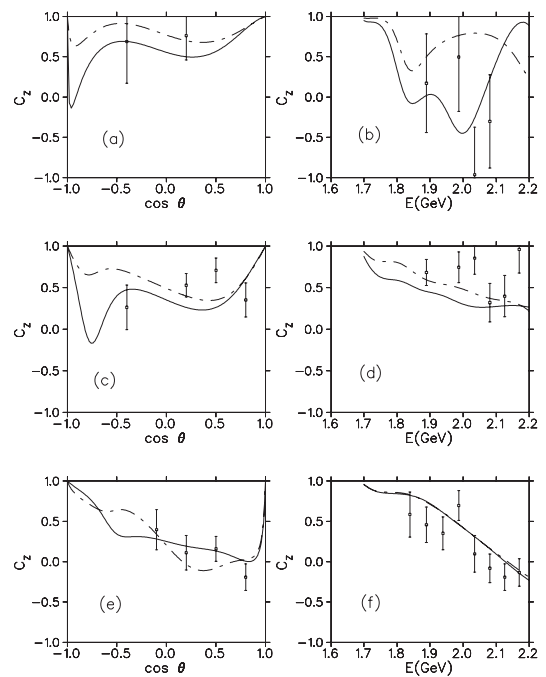


FIG. 6. Double polarization parameter C_Z vs. $\cos \theta_{c.m.}$ for (a) $E_{c.m.} = 1.787$, (c) $E_{c.m.} = 1.939$, and (e) $E_{c.m.} = 2.126$ GeV; double polarization parameter C_Z vs. $E_{c.m.}$ for (b) $\cos \theta_{c.m.} = -0.7$, (d) $\cos \theta_{c.m.} = -0.1$, and (f) $\cos \theta_{c.m.} = 0.8$. The solid curves were obtained with the fit described here and the dot-dashed curves with fit 2 of Ref. [18]. Data are from Ref. [21].

while the electroproduction data have been fit up to a $K\Sigma$ c.m. energy of 2.3 GeV and $-q^2$ value of 3.5 GeV².

The fit parameters consist of the products of the coupling strengths at the electromagnetic and strong interaction vertices, as well as the form factor parameters defined in Sec. II, for all the resonances incorporated in the fit. In addition, the form factor parameters associated with the u - and t -channel Born terms are also included in the fit. Explicit expressions for the coupling constant products can be found in Ref. [18].

For the Born term couplings, fixed values are employed based on empirical data and symmetry relations. The particular values employed here are the same as those used in Ref. [18], and the reader is referred to that reference for those values and a detailed discussion of their determination.

The incorporation of electromagnetic form factors more than doubles the number of parameters required to fit the electroproduction data, as compared with the photoproduction data, and motivated a two step fitting procedure that was used previously in the Λ electroproduction studies of Refs. [27,28]. Using the coupling products obtained in the photoproduction fit of Ref. [18], an initial set of form factor parameters was generated by fitting the electroproduction data with fixed coupling products. Then, with the form factors fixed, the coupling products were adjusted to fit the combined set of photoproduction and electroproduction data. Finally, the resulting coupling products were used in a new fit to the electroproduction data obtained by readjusting the form factor

parameters. In practice this procedure converges quite well after just three or four iterations.

IV. RESULTS AND DISCUSSION

The coupling constant products obtained from the fit described above are listed in Table II. For comparison, the corresponding products from fit 2 of Ref. [18], which is a fit of photoproduction data from the threshold up to 2.2 GeV, are also listed. An examination of the two columns of numerical values in the table reveals that most of the coupling products are similar in the two fits, but there are some significant differences. The form factor parameters obtained in the present fit are listed in Table III.

Results obtained from the fit for the photoproduction observables are shown in Figs. 2–6. In each of these figures, the left side panels display angular distributions at particular c.m. energies, while the right hand panels display energy distributions at particular angles. For comparison, results obtained with fit 2 of Ref. [18] are also exhibited. Note that the cross sections in Fig. 2 have been multiplied by a factor of 10 so as to have units of 10⁻⁵ b/sr.

As a comparison of the solid and dot-dashed curves in these figures indicates, the two fits generally reproduce the photoproduction data with comparable quality. In some cases, the fit of Ref. [18] is better, for example, at the low energy end of the cross section energy distribution for backward angles [Fig. 2(b)]; while in other cases, the present fit is better, for ex-

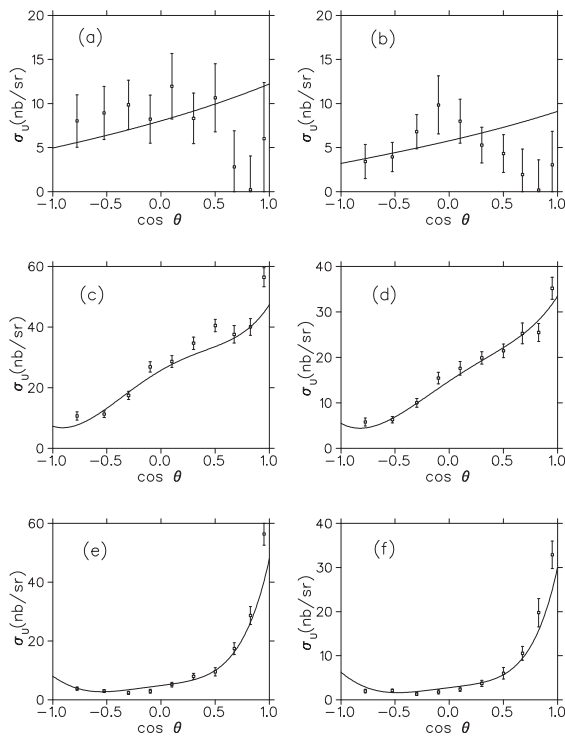


FIG. 7. σ_U vs. $\cos \theta$ for (a) $W = 1.695$ and $-q^2 = 1.80$, (b) $W = 1.695$ and $-q^2 = 2.60$, (c) $W = 1.975$ and $-q^2 = 1.80$, (d) $W = 1.975$ and $-q^2 = 2.60$, (e) $W = 2.275$ and $-q^2 = 1.80$, and (f) $W = 2.275$ GeV and $-q^2 = 2.60$ GeV². All results were obtained with $E_{\text{lab}} = 5.499$ GeV. Data are from Ref. [30].

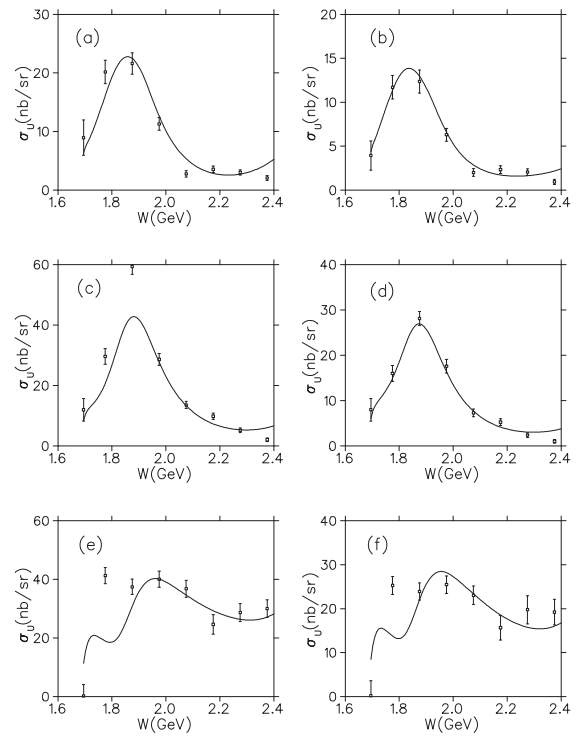


FIG. 8. σ_U vs. W for (a) $\cos \theta = -0.525$ and $-q^2 = 1.80$, (b) $\cos \theta = -0.525$ and $-q^2 = 2.60$, (c) $\cos \theta = 0.1$ and $-q^2 = 1.80$, (d) $\cos \theta = 0.1$ and $-q^2 = 2.60$, (e) $\cos \theta = 0.825$ and $-q^2 = 1.80$, and (f) $\cos \theta = 0.825$ and $-q^2 = 2.60$ GeV². All results were obtained with $E_{\text{lab}} = 5.499$ GeV. Data are from Ref. [30].

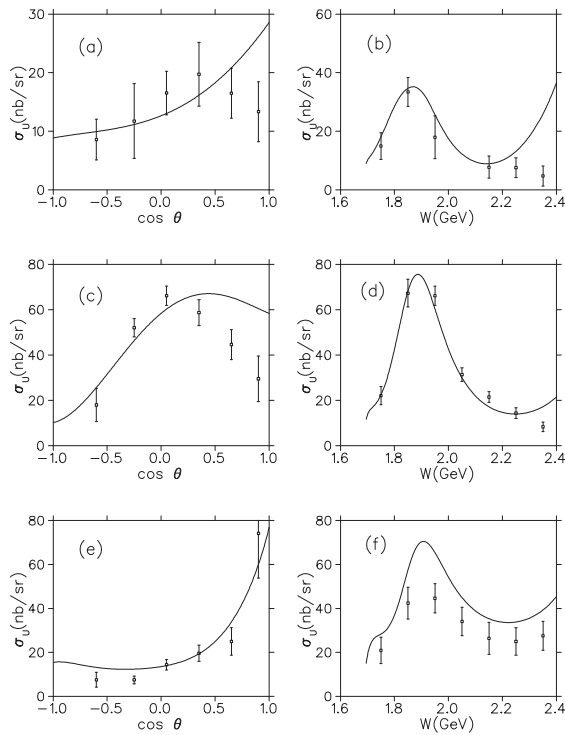


FIG. 9. σ_U vs. $\cos\theta$ for (a) $W = 1.725$, (c) $W = 1.950$, and (e) $W = 2.250$ GeV; σ_U vs. W for (b) $\cos\theta = -0.6$, (d) $\cos\theta = 0$, and (f) $\cos\theta = 0.65$. All results were obtained with $-q^2 = 1.00$ GeV² and $E_{\text{lab}} = 4.056$ GeV. Data are from Ref. [29].

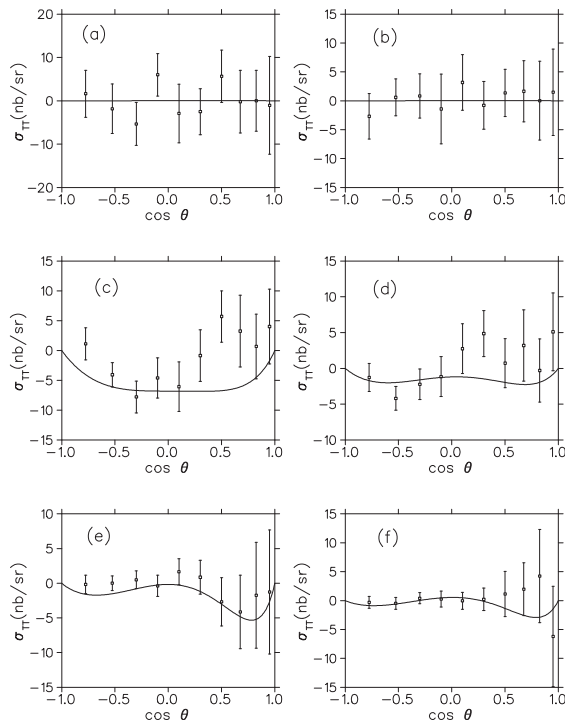


FIG. 10. σ_{TT} vs. $\cos\theta$ for (a) $W = 1.695$ and $-q^2 = 1.80$, (b) $W = 1.695$ and $-q^2 = 2.60$, (c) $W = 1.975$ and $-q^2 = 1.80$, (d) $W = 1.975$ and $-q^2 = 2.60$, (e) $W = 2.275$ and $-q^2 = 1.80$, and (f) $W = 2.275$ GeV and $-q^2 = 2.60$ GeV². All results were obtained with $E_{\text{lab}} = 5.499$ GeV. Data are from Ref. [30].

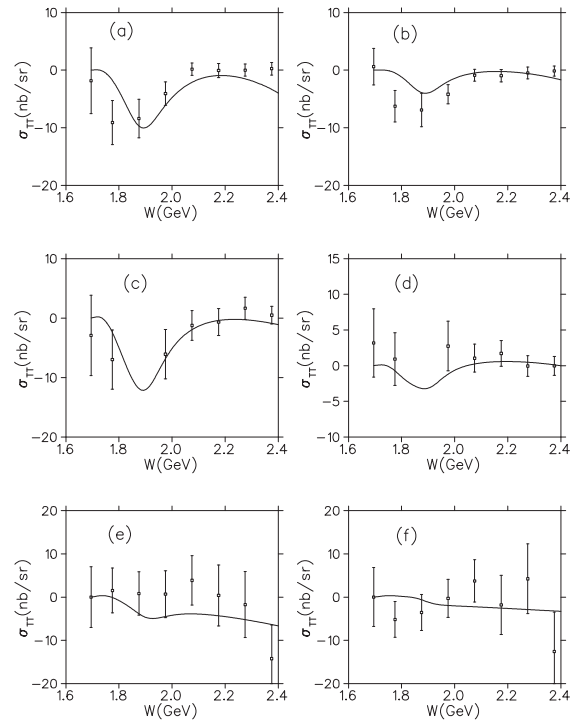


FIG. 11. σ_{TT} vs. W for (a) $\cos\theta = -0.525$ and $-q^2 = 1.80$, (b) $\cos\theta = -0.525$ and $-q^2 = 2.60$, (c) $\cos\theta = 0.1$ and $-q^2 = 1.80$, (d) $\cos\theta = 0.1$ and $-q^2 = 2.60$, (e) $\cos\theta = 0.825$ and $-q^2 = 1.80$, and (f) $\cos\theta = 0.825$ and $-q^2 = 2.60$ GeV². All results were obtained with $E_{\text{lab}} = 5.499$ GeV. Data are from Ref. [30].

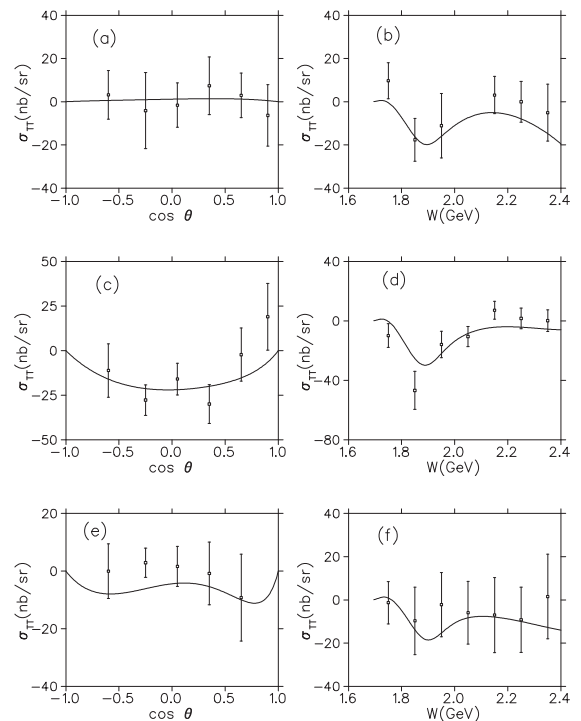


FIG. 12. σ_{TT} vs. $\cos\theta$ for (a) $W = 1.725$, (c) $W = 1.950$, and (e) $W = 2.250$ GeV; σ_{TT} vs. W for (b) $\cos\theta = -0.6$, (d) $\cos\theta = 0$, and (f) $\cos\theta = 0.65$. All results were obtained with $-q^2 = 1.00$ GeV² and $E_{\text{lab}} = 4.056$ GeV. Data are from Ref. [29].

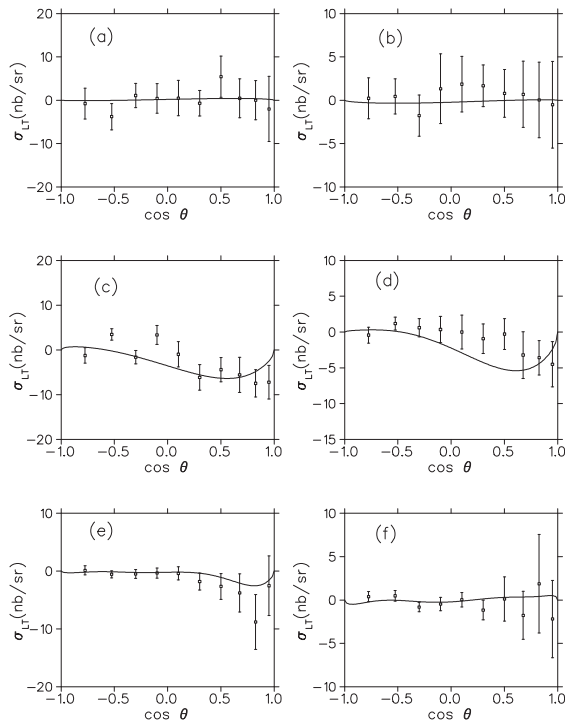


FIG. 13. σ_{LT} vs. $\cos\theta$ for (a) $W = 1.695$ and $-q^2 = 1.80$, (b) $W = 1.695$ and $-q^2 = 2.60$, (c) $W = 1.975$ and $-q^2 = 1.80$, (d) $W = 1.975$ and $-q^2 = 2.60$, (e) $W = 2.275$ and $-q^2 = 1.80$, and (f) $W = 2.275$ GeV and $-q^2 = 2.60$ GeV². All results were obtained with $E_{\text{lab}} = 5.499$ GeV. Data are from Ref. [30].

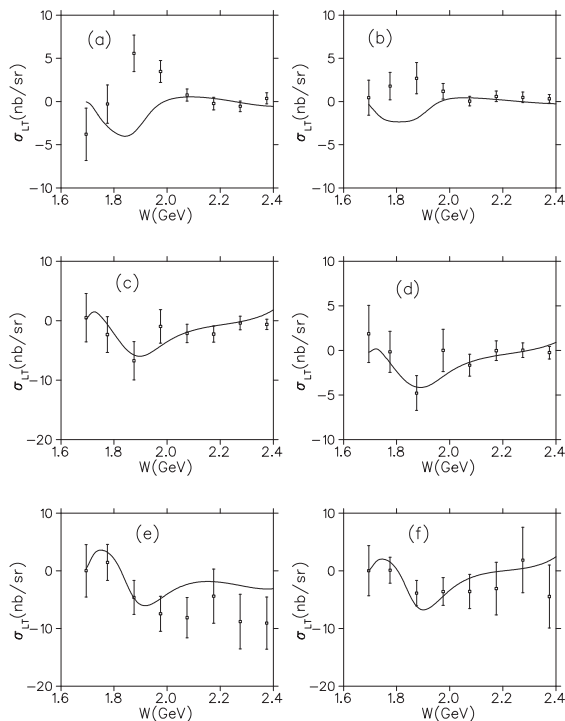


FIG. 14. σ_{LT} vs. W for (a) $\cos\theta = -0.525$ and $-q^2 = 1.80$, (b) $\cos\theta = -0.525$ and $-q^2 = 2.60$, (c) $\cos\theta = 0.1$ and $-q^2 = 1.80$, (d) $\cos\theta = 0.1$ and $-q^2 = 2.60$, (e) $\cos\theta = 0.825$ and $-q^2 = 1.80$, and (f) $\cos\theta = 0.825$ and $-q^2 = 2.60$ GeV². All results were obtained with $E_{\text{lab}} = 5.499$ GeV. Data are from Ref. [30].

ample, in the angular distribution of the hyperon recoil asymmetry at low energies [Fig. 3(a)]. For some observables and over some kinematic ranges, the quality of the data is not good enough to clearly distinguish between the fits. This is particularly true of the double polarization observables (Figs. 5 and 6).

The remaining 11 figures display results obtained with the present fit for the virtual photoproduction structure functions. The first of these figures, Fig. 7, displays σ_U angular distributions for several values of the $K\Sigma$ c.m. energy and two different values of $-q^2$. Energy distributions for the same structure function are shown in Fig. 8. In both figures, the data points are from the most recent CLAS electroproduction experiment [30]. The fit generally does a good job reproducing the data for this structure function, except that there appears to be some structure in the angular distribution data at lower energies that is not seen in the fit [Figs. 7(a) and 7(b)], and for forward angles, the fit appears to fall below the empirical energy distributions at the low energy end [Figs. 8(e) and 8(f)].

A comparison of the calculated σ_U for $-q^2 = 1.00$ GeV² with older CLAS data [29] is shown in Fig. 9. In this figure, the left hand panels display angular distributions, while the right hand panels display energy distributions. The agreement with the data at this value of $-q^2$ is not quite as good as in Figs. 7 and 8, but with some exceptions, the calculated distributions do reproduce the general trends seen in the empirical distributions.

Results for the structure function σ_{TT} are shown in the next three figures. The data points in Figs. 10 and 11 are from the more recent CLAS experiment [30], while the data points in Fig. 12 are from the older CLAS experiment [29].

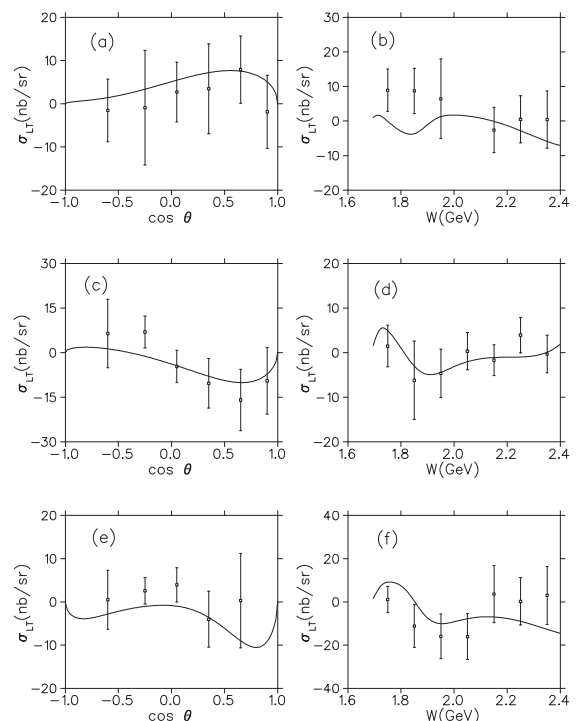


FIG. 15. σ_{LT} vs. $\cos\theta$ for (a) $W = 1.725$, (c) $W = 1.950$, and (e) $W = 2.250$ GeV; σ_{LT} vs. W for (b) $\cos\theta = -0.6$, (d) $\cos\theta = 0$, and (f) $\cos\theta = 0.65$. All results were obtained with $-q^2 = 1.00$ GeV² and $E_{\text{lab}} = 4.056$ GeV. Data are from Ref. [29].

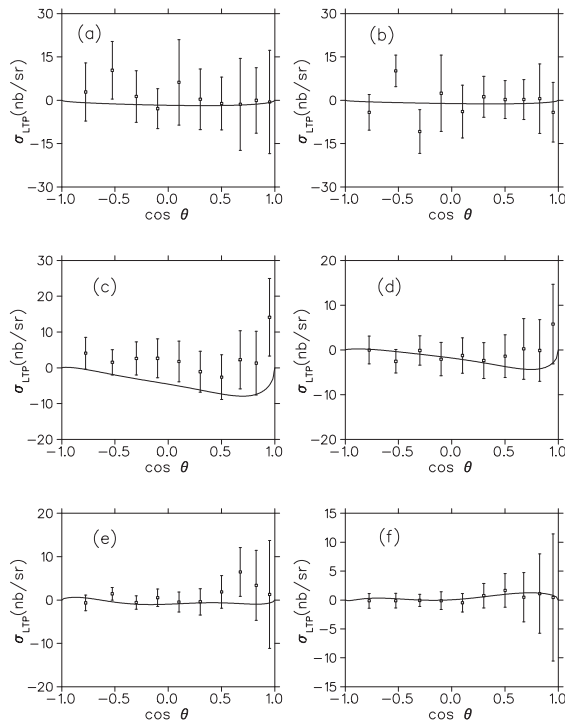


FIG. 16. $\sigma_{LT'}$ vs. $\cos\theta$ for (a) $W = 1.695$ and $-q^2 = 1.80$, (b) $W = 1.695$ and $-q^2 = 2.60$, (c) $W = 1.975$ and $-q^2 = 1.80$, (d) $W = 1.975$ and $-q^2 = 2.60$, (e) $W = 2.275$ and $-q^2 = 1.80$, and (f) $W = 2.275$ GeV and $-q^2 = 2.60$ GeV². All results were obtained with $E_{\text{lab}} = 5.499$ GeV. Data are from Ref. [30].

As for σ_U , the calculated σ_{TT} generally reproduces the data quite well. At intermediate energies, the forward parts of the angular distributions seem to be a little too low [Figs. 10(c) and 10(d)], but the error bars are large enough to make this conclusion uncertain.

Corresponding results for the structure function σ_{LT} are exhibited in Figs. 13–15. As for the σ_{TT} results, the first two of these figures provide a comparison of the calculated angular and energy distributions with the more recent CLAS data, while the third figure provides a comparison with the older CLAS data. Once again, the calculated structure function reproduces the data quite well. The only difficulties are in the angular distributions at intermediate energies, where the calculated structure function may be a little low over parts of the angular range [Figs. 13(c) and 13(d)], and at the low energy end of the energy distributions for backward angles, where the energy dependence of the calculated structure function is incorrect [Figs. 14(a) and 14(b)].

Finally, Figs 16 and 17 depict the calculated angular and energy distributions, respectively, of the structure function $\sigma_{LT'}$ (which appears as σ_{LTP} on the vertical axes of the panels). In both of these figures, the data points are from the more recent CLAS experiment [30]. While the calculated structure functions are a little low at certain energies and angles, the trends of the empirical distributions are generally well reproduced.

In summary, a new fit has been obtained for the electromagnetic production of Σ^0 from the proton using a tree-

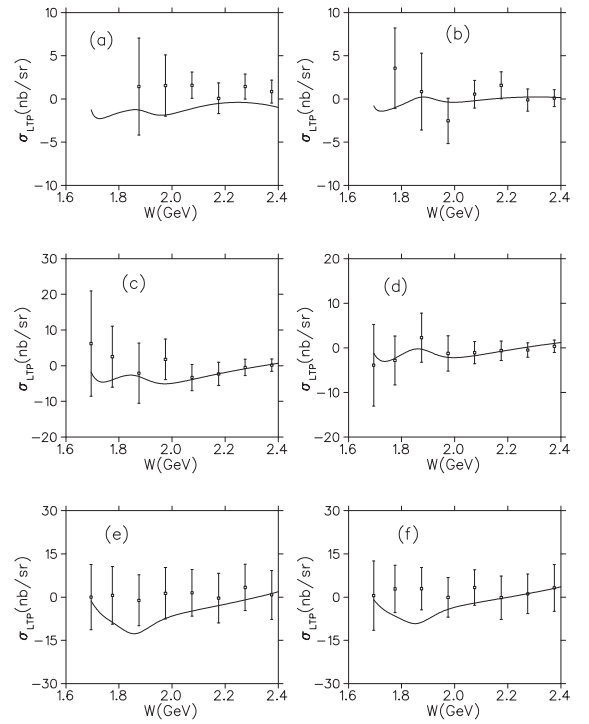


FIG. 17. $\sigma_{LT'}$ vs. W for (a) $\cos\theta = -0.525$ and $-q^2 = 1.80$, (b) $\cos\theta = -0.525$ and $-q^2 = 2.60$, (c) $\cos\theta = 0.1$ and $-q^2 = 1.80$, (d) $\cos\theta = 0.1$ and $-q^2 = 2.60$, (e) $\cos\theta = 0.825$ and $-q^2 = 1.80$, and (f) $\cos\theta = 0.825$ and $-q^2 = 2.60$ GeV². All results were obtained with $E_{\text{lab}} = 5.499$ GeV. Data are from Ref. [30].

level effective Lagrangian model similar to that employed previously to study the electromagnetic production of Λ 's from the proton. In the s channel, the model incorporates most of the well-established nucleon and Δ resonances with spins up to $\frac{5}{2}$, as well as three less well-established nucleon resonances of higher energy. It also includes a variety of hyperon resonances in the u channel and two kaon resonances in the t channel. Form factors, similar to those employed in earlier fits to the electroproduction of Λ 's, have been included at the electromagnetic vertices. The model has been used to fit data for both the photoproduction reaction, $\gamma p \rightarrow K^+ \Sigma^0$, and the electroproduction reaction, $ep \rightarrow e' K^+ \Sigma^0$, over a wide kinematic range. The fit to the photoproduction data is comparable to that reported earlier in Ref. [18]. With a few exceptions, the fit to the electroproduction data reproduces the empirical observables quite well over the full kinematic range considered.

The fit described here is subject to the usual limitations of fits based on tree-level effective Lagrangian models. Since the parameters associated with the s -, u -, and t -channel resonances are varied independently of one another, the fits are not explicitly unitary. In addition, no attempt has been made to take account of possible coupling with other outgoing channels, such as the $K^0 \Sigma^+$ channel. Finally, because the success of the fit depends on a rather delicate balancing of a fairly large number of parameters, it cannot be reliably used outside the fitted energy range.

- [1] H. Thom, E. Gabathuler, D. Jones, B. D. McDaniel, and W. M. Woodward, *Phys. Rev. Lett.* **11**, 433 (1963); M. Grilli, L. Mezzetti, M. Nigro, and E. Schiavuta, *Nuovo Cim.* **38**, 1467 (1965); H. Thom, *Phys. Rev.* **151**, 1322 (1966); D. E. Groom and J. H. Marshall, *ibid.* **159**, 1213 (1967); T. Fujii *et al.*, *Phys. Rev. D* **2**, 439 (1970).
- [2] F. M. Renard and Y. Renard, *Nucl. Phys. B* **1**, 389 (1967); *Phys. Lett. B* **24**, 159 (1967); **25**, 490 (1971); Y. Renard, *ibid.* **40**, 499 (1972).
- [3] R. A. Adelseck, C. Bennhold, and L. E. Wright, *Phys. Rev. C* **32**, 1681 (1985); R. A. Adelseck and L. E. Wright, *ibid.* **38**, 1965 (1988); R. A. Adelseck and B. Saghai, *ibid.* **42**, 108 (1990).
- [4] T. Mart, C. Bennhold, and C. E. Hyde-Wright, *Phys. Rev. C* **51**, R1074 (1995); T. Mart and C. Bennhold, *Nucl. Phys. A* **639**, 237c (1998); H. Haberzettl, C. Bennhold, and T. Mart, *ibid.* **684**, 475 (2001).
- [5] T. Mizutani, C. Fayard, G.-H. Lamot, and B. Saghai, *Phys. Rev. C* **58**, 75 (1998).
- [6] M. K. Cheoun, B. S. Han, B. G. Yu, and Il-Tong Cheon, *Phys. Rev. C* **54**, 1811 (1996); Bong Son Han, Myung Ki Cheoun, K. S. Kim, and Il-Tong Cheon, *Nucl. Phys. A* **691**, 713 (2001).
- [7] S. S. Hsiao, D. H. Lu, and Shin Nan Yang, *Phys. Rev. C* **61**, 068201 (2000).
- [8] Wen Tai Chiang, F. Tabakin, T.-S. H. Lee, and B. Saghai, *Phys. Lett. B* **517**, 101 (2001).
- [9] Stijn Janssen, Jan Ryckebusch, Wim Van Nespen, Dimitri Debruyne, and Tim Van Cauteren, *Eur. Phys. J. A* **11**, 105 (2001); Stijn Janssen, Jan Ryckebusch, Dimitri Debruyne, and Tim Van Cauteren, *Phys. Rev. C* **65**, 015201 (2001); **66**, 035202 (2002); S. Janssen, J. Ryckebusch, and T. Van Cauteren, *ibid.* **67**, 052201(R) (2003); S. Janssen, D. G. Ireland, and J. Ryckebusch, *Phys. Lett. B* **562**, 51 (2003).
- [10] Robert A. Williams, Chueng-Ryon Ji, and Stephen R. Cotanch, *Phys. Rev. C* **46**, 1617 (1992).
- [11] J. C. David, C. Fayard, G. H. Lamot, and B. Saghai, *Phys. Rev. C* **53**, 2613 (1996).
- [12] H. Haberzettl, C. Bennhold, T. Mart, and T. Feuster, *Phys. Rev. C* **58**, R40 (1998); T. Mart and C. Bennhold, *ibid.* **61**, 012201 (1999); T. Mart, *ibid.* **90**, 065202 (2014).
- [13] M. Vanderhaeghen, M. Guidal, and J.-M. Laget, *Phys. Rev. C* **57**, 1454 (1998); M. Guidal, J.-M. Laget, and M. Vanderhaeghen, *ibid.* **61**, 025204 (2000); **68**, 058201 (2003).
- [14] Zhenping Li, *Phys. Rev. C* **52**, 1648 (1995); Zhenping Li, Ma Wei-Hsing, and Zhang Lin, *ibid.* **54**, R2171 (1996).
- [15] A. Usov and O. Scholten, *Phys. Rev. C* **72**, 025205 (2005).
- [16] A. V. Sarantsev, V. A. Nikonov, A. V. Anisovich, E. Klempt, and U. Thoma, *Eur. Phys. J. A* **25**, 441 (2005); A. V. Anisovich, R. Beck, E. Klempt, V. A. Nikonov, A. V. Anisovich, and U. Thoma, *ibid.* **48**, 88 (2012).
- [17] Xu Cao, V. Shklyar, and H. Lenske, *Phys. Rev. C* **88**, 055204 (2013).
- [18] Oren V. Maxwell, *Phys. Rev. C* **92**, 044614 (2015).
- [19] J. W. C. McNabb *et al.*, *Phys. Rev. C* **69**, 042201 (2004).
- [20] R. Bradford *et al.*, *Phys. Rev. C* **73**, 035202 (2006).
- [21] R. Bradford *et al.*, *Phys. Rev. C* **75**, 035205 (2007).
- [22] B. Dey *et al.*, *Phys. Rev. C* **82**, 025202 (2010).
- [23] A. Lleres *et al.*, *Eur. Phys. J. A* **31**, 79 (2007).
- [24] Oren V. Maxwell, *Phys. Rev. C* **70**, 044612 (2004).
- [25] Oren V. Maxwell, *Phys. Rev. C* **76**, 014621 (2007).
- [26] Alejandro de la Puente, Oren V. Maxwell, and Brian A. Raue, *Phys. Rev. C* **80**, 065205 (2009).
- [27] Oren V. Maxwell, *Phys. Rev. C* **85**, 034611 (2012); **86**, 064612 (2012).
- [28] Oren V. Maxwell, *Phys. Rev. C* **90**, 034605 (2014).
- [29] A. Ambrozewicz *et al.*, *Phys. Rev. C* **75**, 045203 (2007).
- [30] D. S. Carman *et al.*, (CLAS Collaboration) *Phys. Rev. C* **87**, 025204 (2013).
- [31] Particle Data Group, K. A. Olive *et al.*, *Chin. Phys. C* **38**, 090001 (2014).
- [32] M. Gari and W. Krumpelmann, *Z. Phys. A* **322**, 689 (1985); Manfred Gari and W. Krumpelmann, *Phys. Lett. B* **173**, 10 (1986); M. F. Gari and W. Krumpelmann, *Phys. Rev. D* **45**, 1817 (1992).
- [33] F. Cardarelli, I. L. Grach, I. M. Narodetskii, E. Pace, G. Salme, and S. Simula, *Phys. Rev. D* **53**, 6682 (1996).